

Journal of Materials Chemistry A

Accepted Manuscript



This is an *Accepted Manuscript*, which has been through the Royal Society of Chemistry peer review process and has been accepted for publication.

Accepted Manuscripts are published online shortly after acceptance, before technical editing, formatting and proof reading. Using this free service, authors can make their results available to the community, in citable form, before we publish the edited article. We will replace this *Accepted Manuscript* with the edited and formatted *Advance Article* as soon as it is available.

You can find more information about *Accepted Manuscripts* in the [Information for Authors](#).

Please note that technical editing may introduce minor changes to the text and/or graphics, which may alter content. The journal's standard [Terms & Conditions](#) and the [Ethical guidelines](#) still apply. In no event shall the Royal Society of Chemistry be held responsible for any errors or omissions in this *Accepted Manuscript* or any consequences arising from the use of any information it contains.

Cite this: DOI: 10.1039/c0xx00000x

ARTICLE TYPE

www.rsc.org/xxxxxx

Solid oxide fuel cells fueled with reduced Fe/Ti oxide

Jelvehnaz Mirzababaei,^a Liang-Shih Fan^b and Steven S.C. Chuang^{*c}

Received (in XXX, XXX) Xth XXXXXXXXXX 20XX, Accepted Xth XXXXXXXXXX 20XX

DOI: 10.1039/b000000x

5 For the first time, Fe-Ti-O containing pellet, a viable chemical looping particle, was used as a solid fuel for direct contact with the Ni/YSZ anode surface of a solid oxide fuel cell. A maximum power density of 97 mW/cm², corresponding to 84% of that in H₂ fuel, was produced using Fe-Ti-O in an inert Ar gas environment at 750 °C. The Fe-Ti-O pellets were able to generate stable electricity under repeated electrochemical oxidation and hydrogen reduction cycles. Temperature-programmed oxidation/reduction
10 coupled with infrared spectroscopic studies revealed that the oxidation of Fe-Ti-O pellet followed a shrinking core model; the reduction followed a progressive-conversion model. The ability of the Fe-Ti-O pellet to generate electricity on the Ni/YSZ surface can be attributed to its low resistivity (< 17 Ω cm) which allows electron to transport from the electrochemical oxidation sites to the anode surface. This study demonstrated that coupling a SOFC with an external reducer using Fe-Ti-O, an oxygen carrier, is a
15 good candidate for electricity generation.

Broader context

Solid oxide fuel cells have promised for efficient electric power generation from natural gas and coal as well as low CO₂ emission for more than one decade. The cost associated with fuel processing and the complexity of its integration within the fuel cell system has hindered its further development to a practical technology. This study demonstrated a novel approach to operate the solid oxide fuel cell
20 with a reducible solid oxide, which has been served as an excellent chemical looping particle, as a fuel. The unique chemical looping particle is composed of Fe and TiO₂. Its reduced form exhibits low resistivity and produces electricity through its electrochemical oxidation on the anode of the solid oxide fuel cell. The results of this study showed that this novel solid oxide fuel cell technology could couple with a reducer of chemical looping process which is in contact with coal, natural gas, and/or biomass for highly efficient electric power generation.

1. Introduction

25 Conventional coal-fired power generation involves many steps and units: coal combustion, steam generation, steam turbines, and electric generators with a less than 35% overall thermodynamic efficiency. One general concept to increase the efficiency and
30 decrease the carbon footprint in power generation from coal is lowering the number of the steps involved through direct conversion of coal on fuel cells.¹ We have developed a unique SOFC unit, which allows direct generation of electricity from electrochemical oxidation of solid carbon and coal particles in a
35 single step.²⁻⁴ Although this carbon-fuel cell process has a significantly higher theoretically thermodynamic efficiency and lower NO_x and CO₂ emission than coal-fired power generation, solid residues of these fuels including silicates present a
40 challenging issue: fouling of the anode surface as illustrated in Fig. 1a, degrading the fuel cell performance.⁵ The carbon-SOFC unit was extended to investigate the feasibility of using reduced Fe-Ti-O pellets, which has been demonstrated as an excellent oxygen carrier for chemical looping^{6,7}, as a solid fuel for SOFCs

in direct contact with the anode surface, shown in Fig. 1b.

45 Fe-Ti-O carrier can be reduced through the direct contact with solid carbon fuel in an external reducer and then electrochemically oxidized on the anode surface of the solid oxide fuel cell, illustrated in Fig. 1c. This novel scheme could result in power generation with high efficiency and low emission
50 and eliminate fouling of the anode by carbon fuel. Application of iron/iron oxide redox couple as a source of chemical energy has also been reported previously in Fe-air batteries.⁸⁻¹¹ In Fe-air batteries, Fe particles, which are not in a direct contact with the anode surface, react with H₂O to produce H₂ for electrochemical
55 oxidation on the anode of a SOFC, generating electricity during discharge while the reverse step is used in the charging process to produce H₂ for reduction of FeO_x.¹¹

The conventional chemical looping combustion (CLC) process uses oxygen carriers such as Fe-Ti-O to transfer the oxygen from the air to the fuel. Carbonaceous fuel is oxidized to produce CO₂ and H₂O while oxygen carrier is reduced in a reducer reactor. Then, the reduced oxygen carrier is transported to the oxidizer reactor for re-oxidation by air. The overall process offers an
60 efficient and low-cost technology for combustion of

carbonaceous fuels with inherent separation of CO₂ greenhouse gas.¹²⁻¹⁸

Fe-Ti-O oxygen carriers in the pellet form have been demonstrated to maintain a nearly 100% constant activity in 100 oxidation/reduction cycles without attrition.⁶ Excellent mechanical strength of these pellets suggests that the reduced form of them may be electrochemically oxidized on the anode of the carbon-SOFC (*i.e.*, solid oxide fuel cell) without fouling the anode surface. Examination of ΔG (Gibbs free energy difference) and E (reversible voltage at 700 and 800 °C versus standard reversible voltage, E⁰, that is obtained at 25 °C) of a number of oxygen carrier materials in Table 1 revealed that Fe/Fe₂O₃ gives the highest E, comparable to that of H₂ fuel. Fe as a solid fuel to be oxidized into Fe₂O₃ offers greater volumetric energy density than those of gaseous hydrogen and solid coal fuels as presented in Table 2. In addition, both reduced metal and metal oxide forms of Fe possess low toxicity compared with other metals and metal oxides.^{18, 19} The application of reduced Fe-Ti-O as a solid fuel in SOFC offers several advantages over H₂-SOFCs and carbon-SOFCs including lowering the cost and complexity of the system by eliminating the fuel processing unit, easy transport and storage of fuel versus H₂-SOFCs, no fouling and deactivation of the anode compared to carbon-SOFCs, increasing the system efficiency in combined cycle applications such as integration of Fe-Ti-O fueled SOFC with chemical looping reducer (Fig. 1c), recycling of fuel *i.e.*, Fe-Ti-O oxygen carrier can reversibly undergo repeated electrochemical oxidation-reduction cycles to generate electricity on the anode surface of the SOFC.

Table 1 Open circuit voltage and change in Gibbs free energy for different oxygen carriers and H₂ fuel.²⁰⁻²²

	n	- $\Delta G = nFE$ (kJ/mol)		E (V)	
		700°C	800°C	700°C	800°C
2Ni + O ₂ → 2NiO	4	310	290	0.803	0.751
4Cu + O ₂ → 2Cu ₂ O	4	220	200	0.570	0.518
4/3Fe + O ₂ → 2/3Fe ₂ O ₃	4	407	384	1.053	0.996
2Fe + O ₂ → 2FeO	4	405	390	1.049	1.010
3/2Fe + O ₂ → 1/2Fe ₃ O ₄	4	405	390	1.049	1.010
2H ₂ + O ₂ → 2H ₂ O(l)	4	418	408	1.082	1.055

Table 2 Energy density of fuels.²³⁻²⁶

Fuel	Energy density (MJ/m ³)
H ₂ (1atm, 25 °C)	12
Coal	20,400
Iron to iron (II) oxide	39,370
Iron to iron (III) oxide	55,120

This study examined the feasibility of using the reduced Fe-Ti-O looping materials as a fuel for the solid oxide fuel cell as shown in Fig. 1b. The completely reduced Fe-Ti-O was able to be electrochemically oxidized to generate electricity. Fe-Ti-O oxygen carriers were further characterized by temperature-programmed reduction/oxidation and infrared spectroscopy to unravel their redox properties. The results of this study indicate that the integration of the SOFC with chemical looping for electricity generation is technically feasible as shown in Fig. 1c in which the Fe-Ti-O carrier can be reduced by various fuels in a reducer and electrochemically oxidized in the solid oxide fuel cell.

Cite this: DOI: 10.1039/c0xx00000x

ARTICLE TYPE

www.rsc.org/xxxxxx

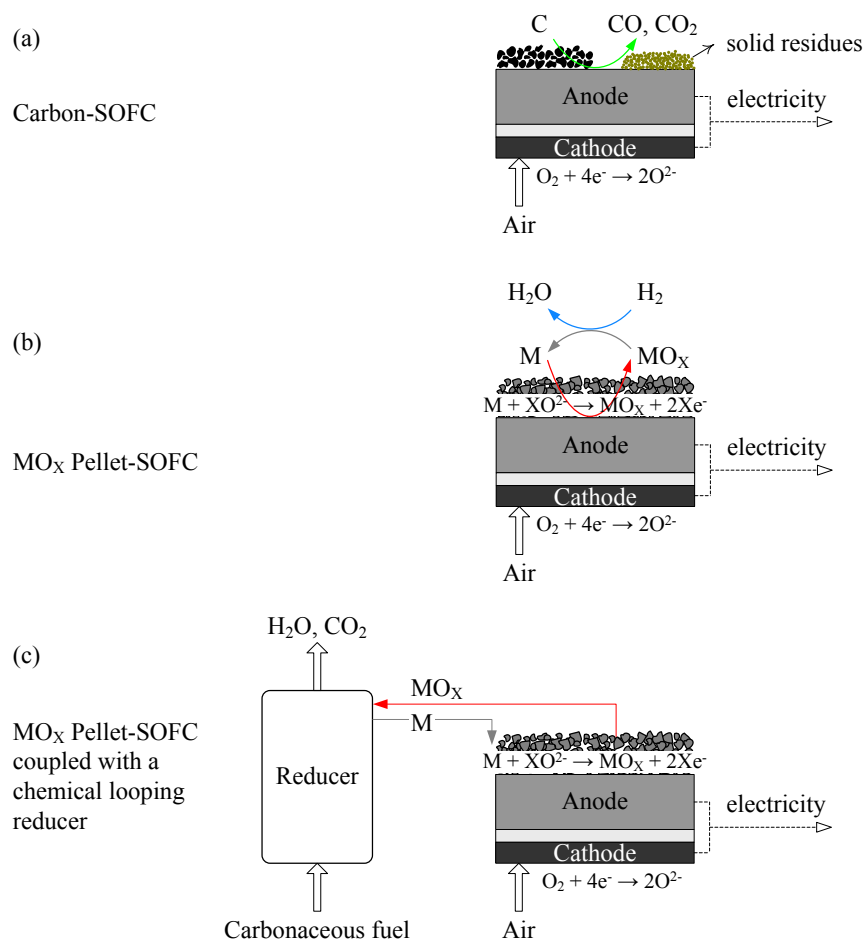


Fig. 1 The schematic of a solid oxide fuel cell operating with (a) solid carbon fuel, (b) solid reduced MO_x (metal oxide), (c) solid reduced MO_x coupled with a chemical looping reducer reactor.

2. Experimental

2.1 Fe-Ti-O preparation

Titania supported iron oxide ($\text{Fe}_2\text{O}_3/\text{TiO}_2$) were prepared using a sol-gel synthesis method as reported elsewhere.²⁷ A solution of 1 g/ml of $\text{FeCl}_3 \cdot 6\text{H}_2\text{O}$ in isopropyl alcohol was mixed with a solution of 1:1 v/v aluminum isopropoxide (Alfa Aesar) in isopropyl alcohol. The mixture was heated to 50 °C to form a gel. The gel was dried under vacuum at 50 °C. The dried gel was then calcined at 500–600 °C in a muffle furnace for 2 h in air. The resulting powder containing 70 wt% Fe_2O_3 was pressed into cylindrical pellets with 5 mm diameter and 1.5–4.5 mm height using a TDP benchtop single-punch tablet press. The pellets were sintered at 900 °C for 12 h.

2.2 Fe-Ti-O characterization

A sealed Diffuse Reflectance Infrared Fourier Transform Spectroscopy (DRIFTS) reactor cell was used for TPR (temperature-programmed reduction) and TPO (temperature-programmed oxidation) studies with 200 mg Fe-Ti-O. Temperature was increased from room temperature to 800 °C at a heating rate of 20 °C/min under Ar/H_2 (20 sccm, 50 vol% H_2) and Ar/O_2 (20 sccm, 50 vol% O_2) flows for TPR and TPO, respectively. The outlet of DRIFTS reactor was connected to a quadrupole mass spectrometer (MS, Pfeiffer Vacuum GSD 301) with a vacuum chamber operating at 5×10^{-6} mbar to monitor the concentration profiles of H_2 and O_2 . The IR spectra were continuously recorded during the process using a Thermo scientific Nicolet 6700 FTIR. The Raman spectra of Fe-Ti-O

powder were obtained at room temperature by a Thermo scientific DXR Raman microscope equipped with a CCD detector and a 780 nm laser before and after redox reactions in DRIFTS cell and on the fuel cell anode. The resistivity of the Fe-Ti-O cylindrical pellets was measured using two-point probe method after (i) reduction in a chemical looping combustion (CLC) reducer reactor at 900 °C, (ii) re-oxidation in a quartz tube under 60 sccm O₂ at 900 °C, and (iii) reduction in a quartz tube under 60 sccm H₂ at 900 °C.

2.3 Fuel cell fabrication

The anode-supported solid oxide fuel cells comprising an anode support, an anode interlayer, an electrolyte layer, a cathode interlayer, and a cathode current collector layer were prepared by the tape casting and screen printing approach similar to our previous work.²⁸ The NiO/3YSZ (3 mol% Y₂O₃ stabilized ZrO₂) 65:35 wt% anode support, NiO/8YSZ/ScSZ (10 mol% Sc₂O₃-1 mol% CeO₂ stabilized ZrO₂) 63:18.5:18.5 wt% anode interlayer, and ScSZ electrolyte layer were produced by tape casting of the slips. The slips were prepared by (i) weighting the oxide powders in the desired amounts, (ii) dispersing the powders in ethanol, (iii) introducing tape casting additives (*i.e.*, pore former for the anode support, binder and dispersant for all slips), and (iv) ball milling the resulting mixture for 24 h. Upon ball milling, the slips were co-casted and dried for 48 h. The anode/electrolyte tapes were cut into 28 mm diameter discs, and fired at 1400 °C. The LSM (La_{0.8}Sr_{0.2}MnO₃)/YSZ 60:40 wt% (Heraeus CL86-8706A) cathode interlayer and the LSM (Heraeus CL86-8706) cathode current collector layer were screen printed on the electrolyte surface with the cathode area of 1.95 cm² and sintered at 1250 and 1100 °C, respectively.

2.4 Fuel cell testing and characterization

The anode-supported fuel cell was tested in an in-house

constructed steel reactor serving as fuel cell housing and anode current collector equipped with a gas inlet port, a feeding unit for Fe-Ti-O powder, and a gas outlet port connected to the MS, as illustrated by a scheme in Fig. 2. This figure also shows SEM micrographs of the SOFC cross-section, which will be discussed in the following section. The fuel cell was sealed to the reactor with an alumina-based sealant and a layer of Ag conductive adhesive (Heraeus C8728) was applied to the surface of the reactor to enhance the current collection at the anode electrode. A Fe-based metal foil was attached to the cathode current collector layer with the aid of Ag conductive adhesive. The cell was placed inside a furnace, heated to 750 °C at a 3 °C/min heating rate, and reduced in Ar/H₂ stream (100 sccm, 50 vol% H₂). Voltage-current characteristics and impedance spectrum of fuel cell were recorded in H₂ fuel with a potentiostat and a frequency response analyzer (Solartron analytical 1470E and 1400 CellTest System). Fe-Ti-O pellets were ground into a fine powder (particle size < 100 μm) and reduced in H₂ at 750 °C before feeding to SOFC. The chemical looping redox reaction was initiated by feeding 2 g of reduced Fe-Ti-O powder to the anode of fuel cell operating at 750 °C under closed circuit condition with an applied voltage of 500 mV in 50 sccm Ar flow. Following electrochemical oxidation of the Fe-Ti-O on the anode, the oxidized powder was regenerated through reduction with H₂ gas flow. In practice, the oxidized Fe-Ti-O would be reduced in a chemical looping reducer reactor through direct contact with carbonaceous fuel at 900 °C. Current profile of the fuel cell and mass over charge (m/e⁻) of gas exhaust were recorded during the redox reactions of Fe-Ti-O in SOFC stack. The fuel cell was cleaned and fractured after testing in H₂ and Fe-Ti-O fuels to be analyzed with scanning electron microscopy (SEM, Hitachi TM-3000) and energy-dispersive X-ray (EDX, Bruker).

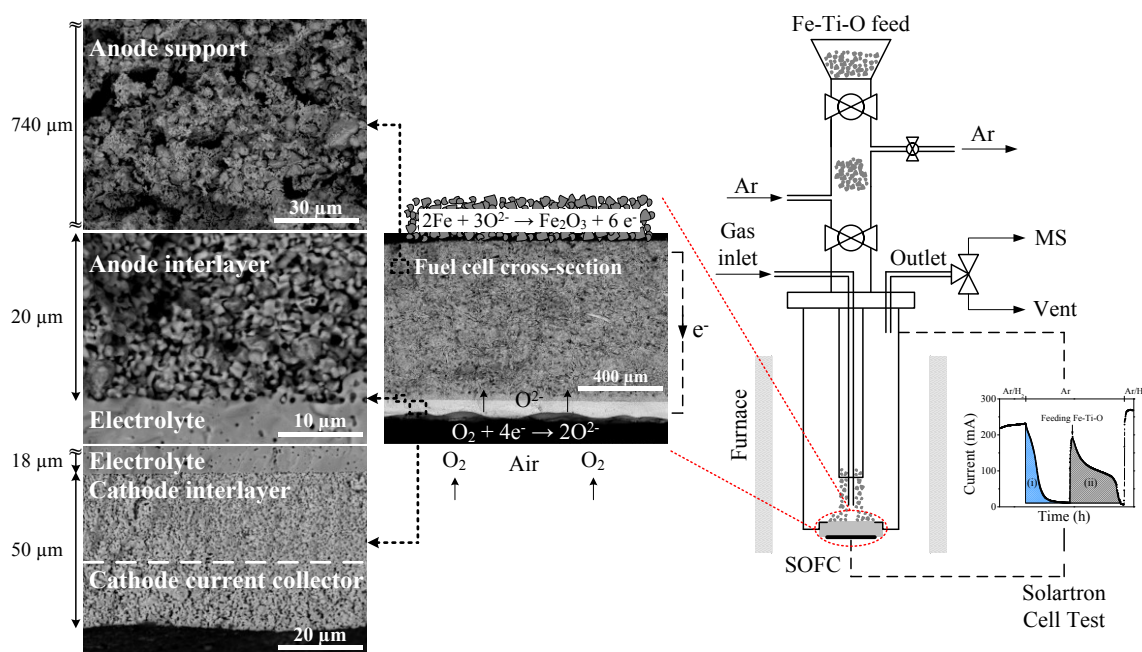


Fig. 2 The scheme of the SOFC testing apparatus and SEM cross-sectional micrograph of different layers of the fuel cell tested with H₂ and Fe-Ti-O fuels.

3. Results and discussion

3.1 Fuel cell structure

Fig. 2 (left) shows the cross-sectional SEM micrographs of the fuel cell tested in H₂ and Fe-Ti-O solid fuel. The SEM of multilayer structure of the fuel cell with a thickness of ca. 830 μm and separate SEM of the anode support, anode interlayer, electrolyte and the cathode are shown in this figure. The 740 μm Ni/3YSZ anode support layer has more porous structure and larger Ni and YSZ particles than the 20 μm Ni/8YSZ anode interlayer. The particle sizes of Ni and YSZ were around 4 and 2.5 μm in the anode support, and 2 and 1 μm in the anode interlayer, respectively. Note that the major function of the anode support is to provide the mechanical strength for the thin anode interlayer, where the electrochemical oxidation of gaseous fuel (e.g. H₂) occurs, and for the thin electrolyte. The 18 μm ScSZ electrolyte was a dense ion conducting membrane separating the anode and the cathode to avoid short-circuit. The 50 μm cathode layer consisted of a less porous LSM/YSZ cathode interlayer and a more porous LSM cathode current collector layer. Porosity of the layers was determined from Archimedes method and pore-sizes were estimated from SEM micrographs. The volumetric three phase boundary (TPB) length for gaseous fuel was estimated from a mathematical model²⁹ for the anode support and anode interlayer. TPB length for the solid fuel was obtained only from the sum of Ni (electronic conductive phase) and YSZ (ionic conductive phase) interfaces on the anode support surface. The parameters needed for TPB calculations were obtained from the cross-sectional and surface SEM micrographs of the fuel cell. Table 3 summarizes the results of physical characterization of the fuel cell.

Table 3 Physical properties of the fuel cell tested in H₂ gaseous fuel and Fe-Ti-O solid fuel

Component	Pore size (μm)	Porosity	v_{L-TPB} (m/m ³)
Anode support surface for solid fuel	-	-	3.3×10^{11}
Anode support for gaseous fuel	0.5-5.5	42% ^a	3.0×10^{12}
Anode interlayer for gaseous fuel	0.25-3.25	30% ^b	7.8×10^{12}

^a estimated from the Archimedes method for the tested fuel cell

^b estimated from the Archimedes method for a half cell, which was comprised only the electrolyte and the anode interlayer

3.2 Temperature-programmed reduction/oxidation with infrared spectroscopy

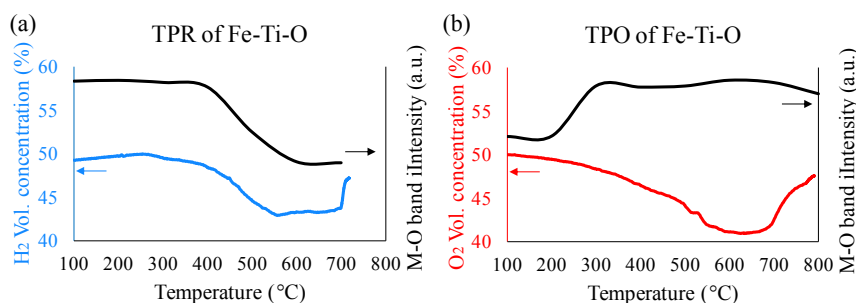


Fig. 3 (a) TPR and (b) TPO of 200 mg Fe-Ti-O powder along with the IR absorbance intensity of M–O band at 800 cm⁻¹ during temperature programming from 100 to 800 °C at a heating rate of 20 °C/min. The M–O intensity was taken from Fig. 4.

Fig. 3 shows the results of temperature-programmed reduction/oxidation (TPR/TPO) along with IR absorbance intensity of the broad band centered at 800 cm⁻¹, which could be attributed to the metal-oxygen (M–O) vibration band of Fe-Ti-O.³⁰ The M–O intensities were obtained from IR spectra in Fig. 4. Fig. 3a shows that the decrease in H₂ concentration began at 400°C. The absorbance intensity of M–O band decreased along with hydrogen consumption, reflecting reduction of the Fe-Ti-O. Reduction temperature of supported iron oxide is known to be higher than that of pure iron oxide due to the interaction of iron oxide with the support.³¹⁻³³ Reduction temperature has also been found to increase with heating rate and the amount of sample.³⁴ Oxygen consumption, illustrated in the TPO profile in Fig. 3b, shows Fe-Ti-O was gradually oxidized with increasing temperature while the M–O intensity exhibited a sharp increase at temperature above 220 °C. These observations suggested that the oxidation occurred on the surface of the Fe-Ti-O particle firstly and then move inward, following the shrinking core model.^{35, 36} Although the DRIFTS study of gas phase oxidation of Fe-Ti-O may not entirely emulate electrochemical oxidation, both oxidation and electrochemical oxidation are expected to involve inward migration and diffusion of oxygen anion.^{37, 38} In contrast, the TPR (i.e., H₂ concentration) profile in parallel to the M–O intensity profile (see Fig. 3a) suggested that the reduction reaction could follow a progressive-conversion model which does not produce a drastic boundary between the oxidized and reduced region inside of the Fe-Ti-O particle. According to progressive-conversion model the reactant gas, which is H₂ in this case, enters and reacts homogeneously throughout the particle causing a gradual variation in reactant concentration within the entire solid particle.³⁶

Cite this: DOI: 10.1039/c0xx00000x

www.rsc.org/xxxxxx

ARTICLE TYPE

Fig. 4 shows the IR absorbance spectra of Fe-Ti-O recorded during TPR and TPO. A decrease in the intensity of M–O band at 1000–600 cm^{-1} range during TPR, shown in Fig. 4a, indicates the depletion of M–O bands. This change can be clearly observed in difference spectra which are shown as c-h T (obtained from subtracting the normalized single beam spectrum

of heating from that of cooling at $T = 300\text{--}800\text{ }^\circ\text{C}$). The c-h 300 spectrum showed a broad negative band at 1000–600 cm^{-1} . The difference spectra exhibited a broad positive band during TPO in Fig. 4b, revealing regeneration of M–O bands through re-oxidation of Fe-Ti-O powder.

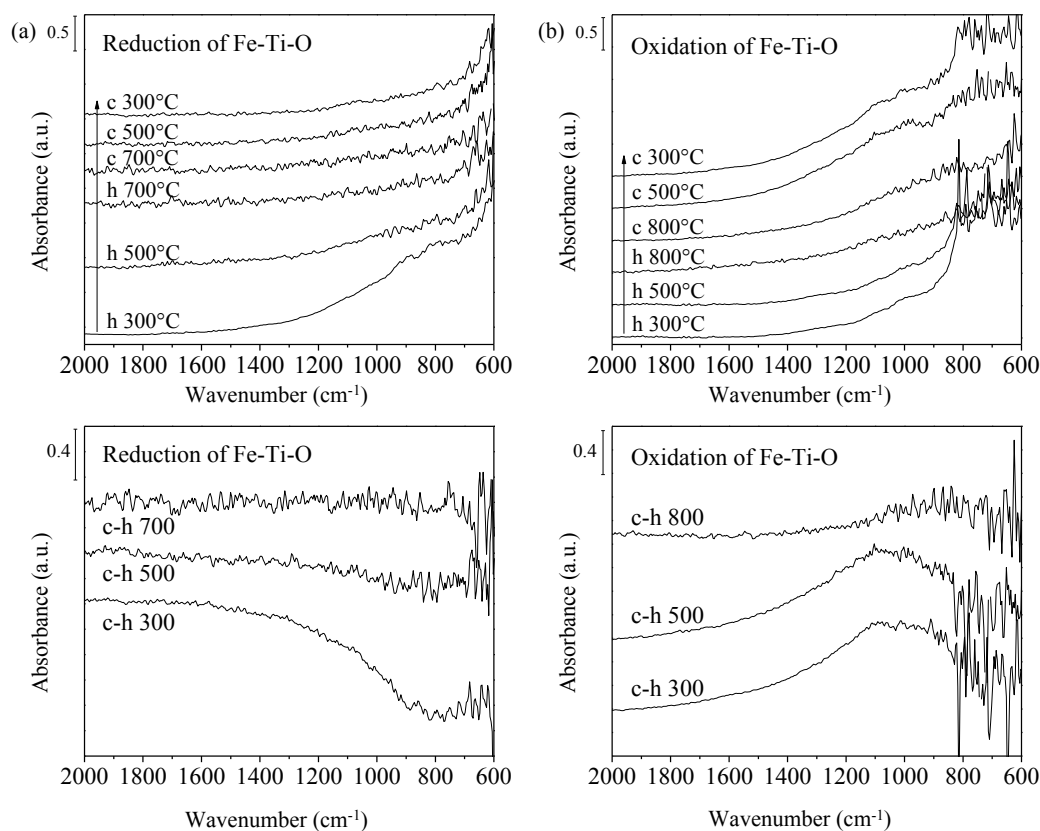
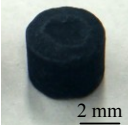
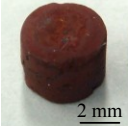
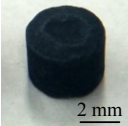
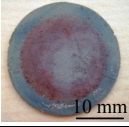


Fig. 4 IR absorbance spectra of Fe-Ti-O powder during (a) TPR and (b) TPO. Top figures show the individual IR absorbance spectra: $-\log(I)$ where I is the single beam spectrum at a certain temperature (300–800 $^\circ\text{C}$) during heating or cooling processes. Bottom figures show the absorbance spectra obtained from $-\log(I_c/I_h)$ where I_c and I_h are normalized single beam spectra during cooling and heating process, respectively. The single beam spectrum in the DRIFTS is equivalent to the transmission IR spectrum when the spectrum of the sample is taken in a transmission mode.

3.3 Resistivity

Table 4 lists the resistivity of the Fe-Ti-O pellets and the fuel cell anode surface. Fe-Ti-O pellets possess low resistivity after reduction in pure H_2 flow at 900 $^\circ\text{C}$. The resistivity of reduced Fe-Ti-O pellets and the Ni/YSZ anode surface are in the same range. As expected, the resistivity of the Fe-Ti-O pellet significantly increased after oxidation in pure O_2 flow at 900 $^\circ\text{C}$. The low resistivity (*i.e.*, high electrical conductivity) of the reduced pellet could play a significant role in ability of the oxygen carrier to conduct the electron from the electrochemical oxidation site to the anode surface.

Table 4 Resistivity results of Fe-Ti-O pellets and fuel cell anode surface before and after redox reactions.

Sample	Redox condition	Resistivity (Ω cm)	Image
Reduced Fe-Ti-O pellet	Reduced in a CLC reducer through direct contact with solid carbon – 900 °C	16.5	
Oxidized Fe-Ti-O pellet	Oxidized in a quartz tube under 60 sccm O ₂ – 900 °C	1.2×10^7	
Reduced Fe-Ti-O pellet	Reduced in a quartz tube under 60 sccm H ₂ – 900 °C	2.4	
Anode surface	Reduced in a SOFC stack under 50 sccm H ₂ – 750 °C	1–3.5	

3.5 Fuel cell performance with H₂ and Fe-Ti-O fuels

Fig. 5 shows voltage-current (V–I) curve and impedance spectrum of the fuel cell at 750 °C in Ar/H₂ (100 sccm, 50 vol% H₂) before introducing Fe-Ti-O solid fuel. The fuel cell exhibited an open circuit voltage (OCV) of 1.01 V and a maximum current density of 555 mA/cm². The low current density compared to a number of literature results³⁹⁻⁴¹ was resulted from the high ohmic resistance (represented by the high frequency intercept of the impedance arc with the X-axis). This high ohmic resistance can be attributed to the use of low-cost Fe-based alloy for current collector which exhibited an electrical resistivity of 0.12 Ω .m at room temperature compared to 1×10^{-7} Ω .m of precious metals such as platinum. A study on various cathode current collectors indicated the effect of utilized current collector on changing the SOFC performance.⁴² The total resistance of the fuel cell (the X value at the lowest frequency of impedance arc) was around 2.8 Ω .cm², consistent with the slope of the V–I curve.

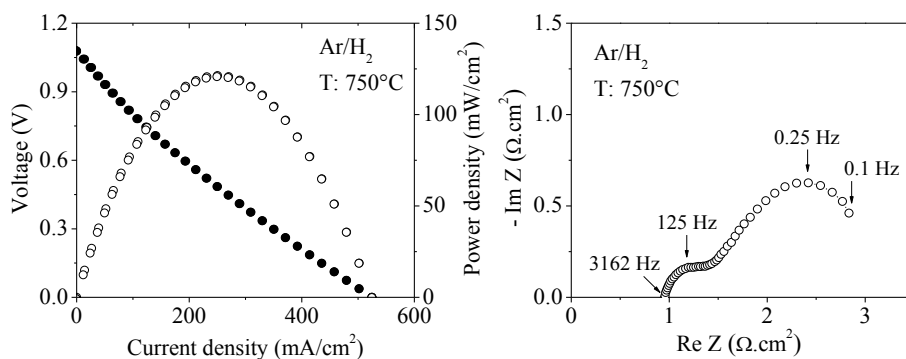
**Fig. 5** Voltage-current curve and impedance spectrum of the fuel cell at 750 °C in Ar/H₂ (100 sccm, 50 vol% H₂).

Fig. 6 shows MS intensity profile of Ar (m/e^- : 40) and H₂ (m/e^- : 2) at the exhaust gas and current density profile of the fuel cell operating with H₂ fuel and then Fe-Ti-O under a constant voltage of 500 mV. Following reduction of Ni/YSZ anode with Ar/H₂ feed, Ar/H₂ was switched to a pure Ar flow. The switch led to a decrease in the current from 235 to 10 mA/cm². The area under the current density decay curve which was produced by residual H₂ is shown as the blue shaded area (i) in Fig. 6. The integrated area (i) multiplied by the constant voltage gives the total electrical work (*i.e.*, energy) generated by residual H₂ in the anode chamber after gas flow switch.

Introducing 2 g of the reduced Fe-Ti-O powder onto the fuel cell anode surface under 500 mV (the voltage that gave the maximum powder density of the fuel cell) generated a current density of 195 mA/cm² and a maximum power density of 97.5 mW/cm², corresponding to 84% of that in H₂ fuel. It is important to note that Fe-Ti-O solid fuel is electrochemically oxidized on the surface of the anode support while hydrogen gaseous fuel mostly in the anode interlayer.³⁹ Three phase boundary (TPB) available in the interlayer for H₂ gaseous fuel was larger than that

on the surface of the anode support for Fe-Ti-O solid fuel. TPBs are reaction sites where ions, electrons and chemical species (gas or solid) meet for electrochemical reaction.^{2, 43} The volumetric TPB length, listed in Table 3, was estimated by a mathematical method²⁹ to be 7.8×10^{12} m/m³ for the anode interlayer. This value is comparable to those reported in literature.^{2, 44-49} The TPB of the anode surface available for Fe-Ti-O oxidation was about 24 times smaller than that of the anode interlayer for H₂ oxidation and yet resulted in a maximum power comparable to 84% of maximum power in H₂.

The electricity generation from Fe-Ti-O indicates that O²⁻ on the anode support surface can reach the reduced Fe-Ti-O particles for electrochemical oxidation to generate electrons which can be transport back to the anode support surface. The current density was gradually declined as the reduced Fe-Ti-O was getting electrochemically oxidized. Flowing Ar/H₂ for 30 min regenerated the oxidized Fe-Ti-O which could be further electrochemically oxidized to produce electricity, as illustrated in shaded area (iii).

Cite this: DOI: 10.1039/c0xx00000x

www.rsc.org/xxxxxx

ARTICLE TYPE

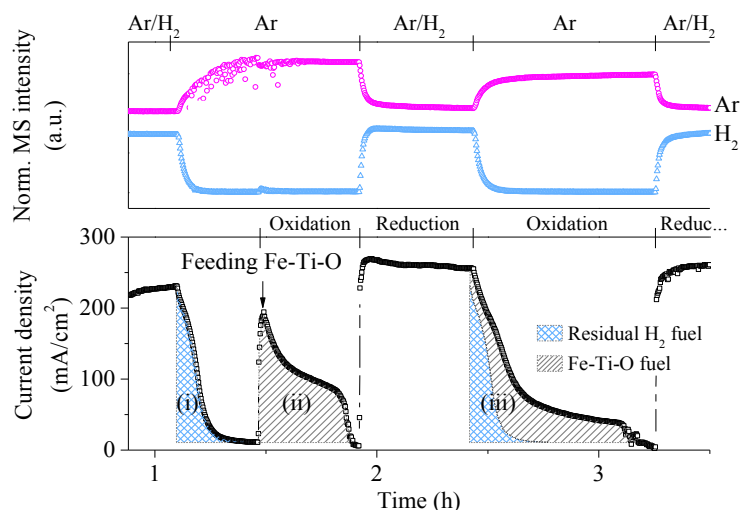
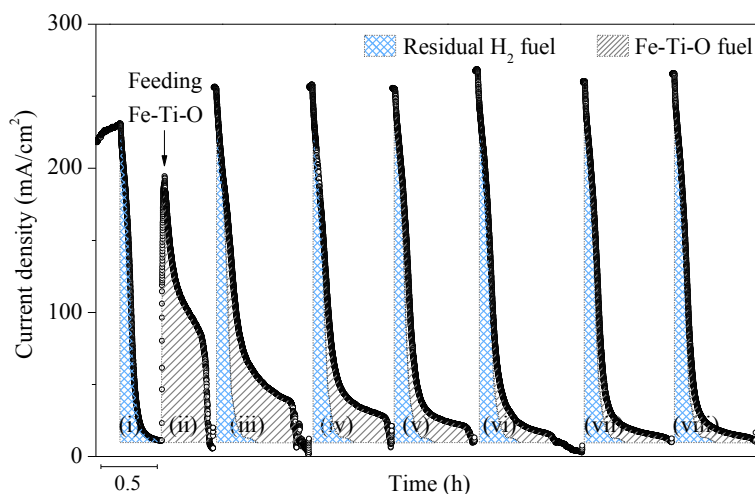


Fig. 6 Concentration profile (MS intensity) of effluent gas and current density profile of the fuel cell under a constant voltage of 500 mV using H₂ and Fe-Ti-O fuels at 750 °C. The shaded areas show the integrated area of the current produced from (i) residual H₂ fuel (after stopping the H₂ flow), H₂ + O²⁻ → H₂O + 2e⁻: blue region; (ii) Fe-Ti-O fuel, 2Fe + 3O²⁻ → Fe₂O₃ + 6e⁻: gray region; and (iii) residual H₂ and Fe-Ti-O fuels together.

5 Fig. 7 shows the current profile of the fuel cell operating with cycling H₂ and Fe-Ti-O. Each cycle involved a reduction step with H₂ and subsequent switching to Ar flow for initiating electrochemical oxidation of Fe-Ti-O. The Fe-Ti-O reduction steps with H₂, similar to those in Fig. 6, are not shown in this

10 figure. It is interesting to note that the current profile, which reflects the kinetics of electrochemical oxidation of Fe-Ti-O, resembles the chemical oxidation profile of a similar material in a TGA study showing iron oxide conversion as a function of time.⁷



15 **Fig. 7** Current density profile of the fuel cell under a constant voltage of 500 mV using H₂ and Fe-Ti-O fuels at 750 °C. The shaded areas show the integrated area of the current peak produced from (i) blue region: residual H₂ fuel (after stopping the H₂ flow); (ii) gray region: Fe-Ti-O fuel; and (iii) to (viii) residual H₂ and Fe-Ti-O together.

20 Fig. 8 summarizes the electrical work produced from oxidation of Fe-Ti-O during each cycle of Fig. 7. The operation of the fuel cell using Fe-Ti-O powder at a constant voltage of 500 mV

produced an electrical work of 73.2 J for the first cycle, corresponding to oxidation of 0.5 mmol of Fe⁰ to Fe³⁺. The conversion of Fe⁰ to Fe³⁺ was estimated to be 18.8% for the first

cycle and this value was decreased for the subsequent cycles and then leveled off. The electrical work was decreased from cycle 1 to 4 and then remained nearly constant. The decrease in electrical work generation after the first cycle can be attributed to the insufficient reduction of Fe-Ti-O. Insufficient reduction could be resulted from the continuous operation of the fuel cell under closed circuit condition, which provided O^{2-} anions to the anode side. The decrease in electrical work is not likely to be resulted from deactivation of Fe-Ti-O since the ability of Fe-Ti-O to retain reactivity for more than 100 cycles has been reported previously in a conventional chemical looping process.²⁷ The low stable

electricity generation after the first few cycles indicated that the extent of Fe-Ti-O reduction and electrochemical oxidation was achieved at the same level.

15 Thermodynamic analysis showed increasing the temperature and hydrogen mole fraction increases the extent of conversion of Fe_2O_3/Fe_3O_4 to Fe/FeO.^{6, 50} The extent of the reduction can be increased by increasing reduction time. The reducer reactor for Fe-Ti-O for a typical chemical looping process usually operates at 900 °C. At this temperature, our Ni/YSZ anode supported cell is expected to exhibit a significantly higher electricity generation than that at 750 °C resulting in higher electrical work generation.

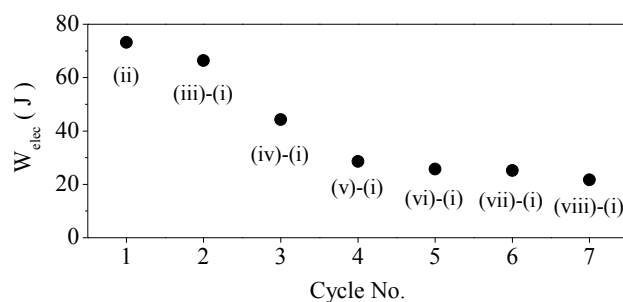


Fig. 8 The electrical work generated by the fuel cell using reduced Fe-Ti-O as fuel at 750 °C in Ar. The electrical work produced during the first cycle was calculated from multiplying the integrated area of the current peak produced from oxidation of Fe-Ti-O by constant voltage; $W_{elec} = E_{const} \int I dt$. The electrical work for the subsequent cycles was estimated by subtraction of the H_2 contribution (blue shaded area (i)) from the total integrated area (shaded area (iii) to (viii)). Blue shaded area (i): integrated area of the current density decay curve produced from residual H_2 fuel; gray shaded area (ii): integrated area of the current peak produced from Fe-Ti-O; (iii) to (viii): integrated area of the current peak produced from residual H_2 and Fe-Ti-O together.

30 The scheme investigated in this study employed the low cost Fe/FeO_x as an oxygen carrier and a well-established Ni/YSZ anode. The overall cost-effectiveness of this new scheme will be governed by two key factors: (i) the stability of Fe/FeO_x in repeated redox cycles and (ii) the maximum powder density of the SOFC. The latter may be further improved by further controlling the porosity of the anode which could minimize the contact issue created by the solid-solid contact on the anode.

3.6 SEM/EDX Characterization

Fig. 9 shows the schematic of the fuel cell reactor and the picture of the fuel cell anode surface along with the corresponding optical microscope (OM) images, SEM images and EDX mappings recorded after the test. The images were taken from two different spots on the anode surface, (a) the center of the

45 anode without deposited Fe-Ti-O, and (b) the near edge of the anode with deposited Fe-Ti-O. The OM and SEM images reveal that the center of the anode support surface, which was right below the gas inlet tube, contains less Fe-Ti-O particles than the rest of the anode region. The TPBs for solid fuel are the Ni (electronic conductive phase) and YSZ (ionic conductive phase) interface which are indicated by the white arrows on the EDX mapping of the clean fuel cell anode surface. The reduced Fe-Ti-O particles that were oxidized to iron oxide on the TPBs are pointed out by red arrows on the EDX mapping of the near edge anode surface. The particle size of Fe-Ti-O needs to be further optimized to create sufficient contact with the anode surface while not depositing on the active sites.

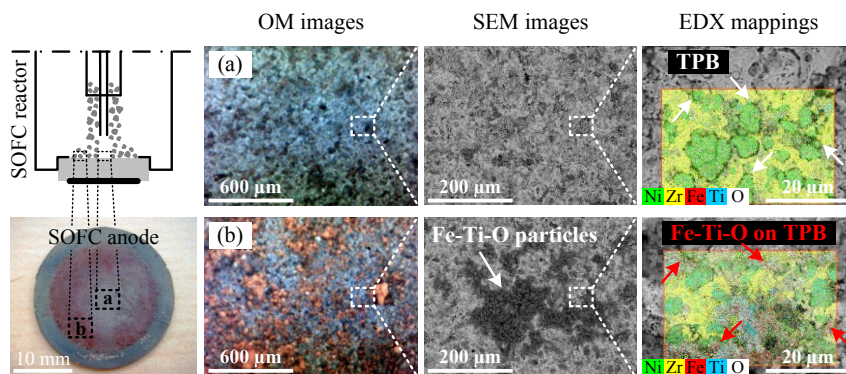


Fig. 9 Schematic of the fuel cell reactor and the picture of the fuel cell anode surface along with the optical microscope (OM) images, SEM images and EDX mappings. The characterization was performed on two different spots of the tested fuel cell anode surface (a) without deposited Fe-Ti-O and (b) with deposited Fe-Ti-O particles.

Cite this: DOI: 10.1039/c0xx00000x

www.rsc.org/xxxxxx

ARTICLE TYPE

3.7 Raman characterization

Fig. 10 shows the Raman spectra of Fe-Ti-O powder under different extent of reduction/oxidation. The Raman spectra of Fe₂O₃ and TiO₂ have been well established⁵¹⁻⁵³ and served as references. The reduced Fe-Ti-O powder with a gray color showed a single small peak associates with TiO₂ support. The color changed to black for the Fe-Ti-O that was reduced on the SOFC anode surface. Fe-Ti-O, which was used as solid fuel and

oxidized on the fuel cell anode under a constant voltage, displays both Fe₂O₃ and TiO₂ peaks as shown in Fig. 10c. The former was produced from electrochemical oxidation of Fe⁰ with O²⁻ anions to generate electricity. The intensities of Fe₂O₃ and TiO₂ peaks increased with the degree of oxidation. Fe-Ti-O powder that was oxidized in a DRIFTS cell under Ar/O₂ flow exhibited a red/orange color. The Raman spectrum of fresh Fe-Ti-O showed the distinct peaks of Fe₂O₃ and TiO₂ with a reddish color.

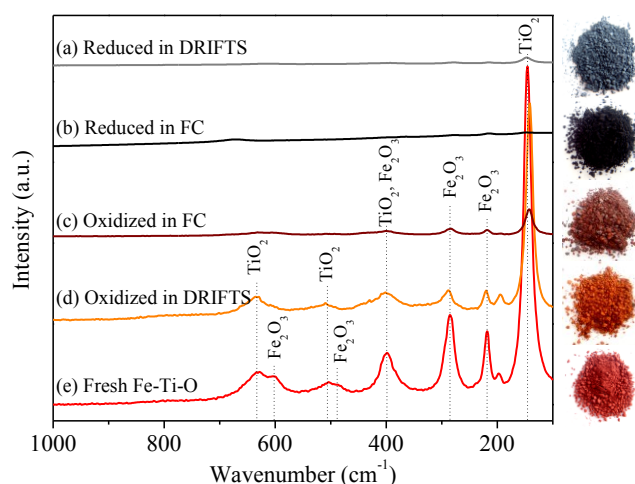


Fig. 10 Raman spectra and pictures of Fe-Ti-O powders that were (a) reduced in a DRIFTS cell flowing Ar/H₂ at 800°C, (b) reduced on the fuel cell anode flowing Ar/H₂ at 750°C, (c) oxidized on the fuel cell anode under a constant voltage flowing Ar at 750°C, (d) oxidized in a DRIFTS cell flowing Ar/O₂ at 800°C, and (e) fresh oxide prior to redox reactions.

4. Conclusions

This study demonstrated that, for the first time, reduced Fe-Ti-O oxygen carrier was electrochemically oxidized on the anode surface of Ni/YSZ anode-supported SOFC for electricity generation. The oxidized Fe-Ti-O can be reduced and further electrochemically oxidized with repeated cycles. Infrared studies showed the M–O bond appeared following oxidation with O₂ and disappeared following reduction with H₂. Coupling the Fe-Ti-O pellet-SOFC with a chemical looping reducer, which uses solid carbon fuel for reduction of Fe-Ti-O, allows the use of solid carbon for electricity generation without its direct contact with the SOFC anode surface, eliminating the anode fouling and degradation. Further economic analysis will be performed to evaluate the cost-competitiveness of this novel concept of SOFCs coupled with an external reducer.

Notes

^a Department of Chemical and Biomolecular Engineering, FirstEnergy Advanced Energy Research Center, The University of Akron, Akron, OH, 44325, USA. E-mail: jm115@ziips.uakron.edu

^b William G. Lowrie Department of Chemical and Biomolecular Engineering, The Ohio State University, 140 West 19th Avenue, Columbus, OH, 43210, USA. E-mail: jan.1@osu.edu

^c Department of Polymer Science, FirstEnergy Advanced Energy Research Center, The University of Akron, Akron, OH, 44325, USA. Fax: +1-330-972-5856; Tel: +1-330-972-6993; E-mail: chuang@uakron.edu

Acknowledgments

This work was financially supported by Ohio Coal Development Office (OCDO), grant no. DE-FG36-06GO86055.

References

1. S. L. Jain, Y. Nabae, B. J. Lakeman, K. D. Pointon and J. T. S. Irvine, *Fuel Cells Bulletin*, 2008, **2008**, 10-13.
2. F. Guzman, R. Singh and S. S. Chuang, *Energy & Fuels*, 2011, **25**, 2179-2186.
3. A. C. Chien and S. S. C. Chuang, *Journal of Power Sources*, 2011, **196**, 4719-4723.

4. T. Siengchum, F. Guzman and S. S. Chuang, *Journal of Power Sources*, 2012, **213**, 375-381.
5. T. M. Gür, *Chemical Reviews*, 2013, **113**, 6179-6206.
6. A. Tong, S. Bayham, M. V. Kathe, L. Zeng, S. Luo and L.-S. Fan, *Applied Energy*, 2014, **113**, 1836-1845.
7. S. C. Bayham, H. R. Kim, D. Wang, A. Tong, L. Zeng, O. McGiveron, M. V. Kathe, E. Chung, W. Wang and A. Wang, *Energy & Fuels*, 2013, **27**, 1347-1356.
8. X. Zhao, Y. Gong, X. Li, N. Xu and K. Huang, *Journal of The Electrochemical Society*, 2013, **160**, A1716-A1719.
9. A. Inoishi, S. Ida, S. Uratani, T. Okano and T. Ishihara, *RSC Advances*, 2013, **3**, 3024-3030.
10. A. Inoishi, S. Ida, S. Uratani, T. Okano and T. Ishihara, *Physical Chemistry Chemical Physics*, 2012, **14**, 12818-12822.
11. N. Xu, X. Li, X. Zhao, J. B. Goodenough and K. Huang, *Energy & Environmental Science*, 2011, **4**, 4942-4946.
12. A. Lyngfelt, *Applied Energy*, 2014, **113**, 1869-1873.
13. J. Adanez, A. Abad, F. Garcia-Labiano, P. Gayan and L. F. de Diego, *Progress in Energy and Combustion Science*, 2012, **38**, 215-282.
14. M. M. Hossain and H. I. de Lasa, *Chemical Engineering Science*, 2008, **63**, 4433-4451.
15. A. Abad, T. Mattisson, A. Lyngfelt and M. Rydén, *Fuel*, 2006, **85**, 1174-1185.
16. R. Siriwardane, H. Tian, G. Richards, T. Simonyi and J. Poston, *Energy & Fuels*, 2009, **23**, 3885-3892.
17. M. E. Boot-Handford, J. C. Abanades, E. J. Anthony, M. J. Blunt, S. Brandani, N. Mac Dowell, J. R. Fernandez, M.-C. Ferrari, R. Gross, J. P. Hallett, R. S. Haszeldine, P. Heptonstall, A. Lyngfelt, Z. Makuch, E. Mangano, R. T. J. Porter, M. Pourkashanian, G. T. Rochelle, N. Shah, J. G. Yao and P. S. Fennell, *Energy & Environmental Science*, 2014, **7**, 130-189.
18. A. Thursfield, A. Murugan, R. Franca and I. S. Metcalfe, *Energy & Environmental Science*, 2012, **5**, 7421-7459.
19. E. R. Monazam, R. W. Breault, R. Siriwardane, G. Richards and S. Carpenter, *Chemical Engineering Journal*, 2013, **232**, 478-487.
20. S. S. Chuang, Catalysis of solid oxide fuel cells. *Catalysis*, The Royal Society of Chemistry: Cambridge, UK, 2005, **18**, 188-189.
21. R. P. O'Hayre, S.-W. Cha, W. Colella and F. B. Prinz, *Fuel cell fundamentals*, John Wiley & Sons New York, 2006.
22. L.-S. Fan, *Chemical looping systems for fossil energy conversions*, Wiley.com, 2011.
23. P. Atkins and J. De Paula, *Elements of physical chemistry*, Oxford University Press, 2013, 82-83.
24. P. J. Reddy, *Clean Coal Technologies for Power Generation*, CRC Press, 2013, 33.
25. C. Toh, *A-Level Practice MCQ Chemistry (Higher 2)*, Step-by-Step International Pte. Ltd., 2013, 2-9.
26. A. Navrotsky, L. Mazeina and J. Majzlan, *Science*, 2008, **319**, 1635-1638.
27. F. Li, H. R. Kim, D. Sridhar, F. Wang, L. Zeng, J. Chen and L.-S. Fan, *Energy & Fuels*, 2009, **23**, 4182-4189.
28. J. Mirzababaei and S. Chuang, *Catalysts*, 2014, **4**, 146-161.
29. V. M. Janardhanan, V. Heuveline and O. Deutschmann, *Journal of Power Sources*, 2008, **178**, 368-372.
30. A. Davydov, *Molecular Spectroscopy of Oxide Catalyst Surfaces*, John Wiley & Sons, 2003, 37-47.
31. H. Y. Lin, Y. W. Chen and C. Li, *Thermochimica Acta*, 2003, **400**, 61-67.
32. X. Gao, J. Shen, Y. Hsia and Y. Chen, *Journal of the Chemical Society, Faraday Transactions*, 1993, **89**, 1079-1084.
33. I. Leith and M. Howden, *Applied catalysis*, 1988, **37**, 75-92.
34. O. Wimmers, P. Arnoldy and J. Moulijn, *The Journal of Physical Chemistry*, 1986, **90**, 1331-1337.
35. J. W. Niemantsverdriet, *Spectroscopy in catalysis*, John Wiley & Sons, 2007, 15-17.
36. O. Levenspiel, *Chemical reaction engineering*, John Wiley & Sons, 1999, 568-569.
37. F. Li, S. Luo, Z. Sun, X. Bao and L.-S. Fan, *Energy & Environmental Science*, 2011, **4**, 3661-3667.
38. F. Li, Z. Sun, S. Luo and L.-S. Fan, *Energy & Environmental Science*, 2011, **4**, 876-880.
39. F. Zhao and A. V. Virkar, *Journal of Power Sources*, 2005, **141**, 79-95.
40. Y. Gong, W. Ji, L. Zhang, B. Xie and H. Wang, *Journal of Power Sources*, 2011, **196**, 928-934.
41. Y. Jiang and A. V. Virkar, *Journal of the Electrochemical Society*, 2001, **148**, A706-A709.
42. S. P. Simner, M. D. Anderson, L. R. Pederson and J. W. Stevenson, *Journal of The Electrochemical Society*, 2005, **152**, A1851-A1859.
43. B. Kenney, M. Valdmanis, C. Baker, J. G. Pharoah and K. Karan, *Journal of Power Sources*, 2009, **189**, 1051-1059.
44. J. R. Wilson, M. Gameiro, K. Mischaikow, W. Kalies, P. W. Voorhees and S. A. Barnett, *Microscopy and Microanalysis*, 2009, **15**, 71.
45. W. Zhu, D. Ding and C. Xia, *Electrochemical and Solid-State Letters*, 2008, **11**, B83-B86.
46. J. R. Wilson and S. A. Barnett, *Electrochemical and Solid-State Letters*, 2008, **11**, B181-B185.
47. J. R. Wilson, W. Kobsiriphat, R. Mendoza, H.-Y. Chen, J. M. Hiller, D. J. Miller, K. Thornton, P. W. Voorhees, S. B. Adler and S. A. Barnett, *Nature materials*, 2006, **5**, 541-544.
48. G. J. Nelson, K. N. Grew, J. R. Izzo Jr, J. J. Lombardo, W. M. Harris, A. Faes, A. Hessler-Wyser, J. Van herle, S. Wang, Y. S. Chu, A. V. Virkar and W. K. S. Chiu, *Acta Materialia*, 2012, **60**, 3491-3500.
49. A. Modjtahedi, N. Hedayat and S. S. C. Chuang, *Solid State Ionics*, 2014, **268, Part A**, 15-22.
50. J. E. Readman, A. Olafsen, Y. Larring and R. Blom, *Journal of Materials Chemistry*, 2005, **15**, 1931-1937.
51. F. Rull, J. Martinez-Frias and J. A. Rodriguez-Losada, *Journal of Raman Spectroscopy*, 2007, **38**, 239-244.
52. Y.-S. Hu, A. Kleiman-Shwarscstein, A. J. Forman, D. Hazen, J.-N. Park and E. W. McFarland, *Chemistry of Materials*, 2008, **20**, 3803-3805.
53. J. Zhang, M. Li, Z. Feng, J. Chen and C. Li, *The Journal of Physical Chemistry B*, 2006, **110**, 927-935.